

# Upcycling fruit waste into high-performance 3D porous aerogel for dye removal: Experimental and density functional theory study

Downloaded from: https://research.chalmers.se, 2025-11-29 20:40 UTC

Citation for the original published paper (version of record):

Imran, M., Pan, M., Islam, A. et al (2025). Upcycling fruit waste into high-performance 3D porous aerogel for dye removal: Experimental and density functional theory study. Case Studies in Chemical and Environmental Engineering, 11. http://dx.doi.org/10.1016/j.cscee.2025.101238

N.B. When citing this work, cite the original published paper.

research.chalmers.se offers the possibility of retrieving research publications produced at Chalmers University of Technology. It covers all kind of research output: articles, dissertations, conference papers, reports etc. since 2004. research.chalmers.se is administrated and maintained by Chalmers Library

FISEVIER

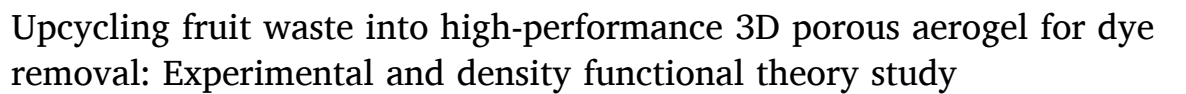
Contents lists available at ScienceDirect

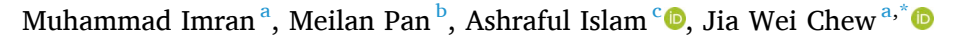
# Case Studies in Chemical and Environmental Engineering

journal homepage: www.sciencedirect.com/journal/case-studies-in-chemicaland-environmental-engineering



# Case Report





- <sup>a</sup> Division of Chemical Engineering, Chalmers University of Technology, 412 96, Gothenburg, Sweden
- b College of Environment, Zhejiang University of Technology, Zhejiang, 310014, China
- c State Key Laboratory of Environmental Aquatic Chemistry, Chinese Academy of Sciences, Haidian District, Beijing, 100085, China

#### ARTICLE INFO

# Keywords: Eco-friendly 3D porous aerogel Green synthesis Dye sorption Biomass waste DFT simulation

#### ABSTRACT

Durian shell waste was subjected to hydrothermal treatment followed by freeze-drying to create highly porous 3D aerogels, whose surfaces were judiciously functionalized to enable strong interactions with RhB dye. The aerogels were tailored to be superhydrophilic/oleophobic to enhance affinity to the dye, magnetic to enable directional mobility, and highly porous (up to 97 %) to augment the specific surface area. The durian shell waste – derived, surface-modified aerogels exhibited RhB removal efficiency of over 99 %. Density Functional Theory (DFT) simulations suggest that the strong adsorption of RhB onto the aerogel was governed by  $\pi$ - $\pi$  interactions, hydrogen bonding, and electrostatic interactions.

# 1. Introduction

Water pollution is a pressing global environmental issue with farreaching consequences, as it severely threatens human health, undermines sustainability efforts, and disrupts the delicate balance of ecosystems. A wide variety of pollutants contaminate water sources, posing significant challenges to water treatment processes. To ensure the safety and quality of water, treatment strategies must be comprehensive, adaptable, and capable of effectively addressing this diverse array of contaminants. This study addresses the treatment of dye-contaminated wastewater, which is generated in substantial volumes by industries such as textiles, dyeing, printing, ink manufacturing, and associated sectors [1].

Dyes are well-characterized pollutants known for their adverse impact on human health and the environment. They are not only toxic and potentially carcinogenic, but also disrupt aquatic ecosystems by limiting light penetration and thus photosynthesis [2]. For example, Rhodamine dye is a highly toxic, non-biodegradable pollutant in industrial effluents, posing severe environmental risks due to its carcinogenic and mutagenic nature [3–5]. Therefore, to ensure that effluent contaminated with Rhodamine dye is treated effectively before disposal, much attention has been dedicated to removing Rhodamine from wastewater utilizing safe, economical, and biodegradable materials [6–8]. Rhodamine dyes encompass several different synthetic

compounds, including Rhodamine B, Rhodamine 6G, Rhodamine 123, Rhodamine 101, etc., with each variant possessing unique chemical properties and thus requiring different treatments [9,10]. To remove Rhodamine B from aqueous solution, Jethave et al. used lead-iron oxide nanoparticles [11], Kooh et al. used Casuarina equisetifolia [12], Suc et al. used activated rice husk ash [13], while Zhang et al. developed an aerogel composite made of co-hybridized 3-dimensional graphene with g-C<sub>3</sub>N<sub>4</sub> and TiO<sub>2</sub> [14]. To remove malachite green and Rhodamine B via adsorption, Datta et al. used a composite made of Fe<sub>3</sub>O<sub>4</sub> and activated carbon [15].

Multiple remediation techniques have been applied to eliminate Rhodamine dye from contaminated water, such as membrane separation [16–18], chemical precipitation [17,19], photocatalysis [20], ion exchange [21], and adsorption [22]. Adsorption-based approaches are considered among the most effective and practical for dye removal from water, because it is economical, simple, adaptable, and highly effective [23]. Carbon-based materials, including carbon nanotubes [24], biochar [25] and graphene (modified graphene oxide or graphene oxide) [26], are especially advantageous for this purpose due to their high surface area and amenability for customization of surface chemistry through different functional groups. Unfortunately, despite their excellent adsorption capacity, the practical use of carbon-based systems is limited in powdered form due to challenges in regeneration and reusability. These drawbacks can be mitigated through the incorporation of

E-mail address: jia.chew@chalmers.se (J.W. Chew).

https://doi.org/10.1016/j.cscee.2025.101238

<sup>\*</sup> Corresponding author.

carbon-based materials into porous, environmentally friendly biomaterials.

As potential scaffolding materials for developing these eco-friendly porous materials, a variety of green and sustainable polymers have been studied, including gelatin [27], cellulose [28], chitosan [29] and starch [30]. Among naturally occurring polymers, cellulose is the most abundant. However, natural cellulose has a low adsorption capacity for contaminants due to the presence of only hydroxyl groups on the surface, and poor water solubility due to strong hydrogen bonds between native cellulose molecules. Incorporating carboxylic groups onto the cellulose surface can increase its capacity for adsorption and water solubility. Adsorbents with exceptional wettability are known to be advantageous for the separation of pollutants from water [18,31], and such surface wettability to polar or non-polar solvents is related to the chemical composition and porous structure of the material [32]. A number of super-wetting materials have been developed for the separation of pollutants from water [33]. For example, Wu et al. designed PU@Fe<sub>3</sub>O<sub>4</sub>@SiO<sub>2</sub>@fluoro sponges for the targeted absorption of non-polar solvents [33]. Unfortunately, the pollutants often cause clogging of the pores and fouling of the material surfaces, limiting the effectiveness of three-dimensional porous structures [34]. The fouling by non-polar solvents may destroy the fine surface architectures of adsorbents, lowering the overall efficiency of pollutant removal. On the other hand, when superhydrophobic adsorbents are used for filtration, their surfaces are in contact with non-polar liquids rather than water, reducing the efficiency of continuous pollutant filtration [35].

Collectively, the past studies suggest that superhydrophilic adsorbents, which can selectively bind to the hydrophilic dye pollutants and repel non-polar liquids, may be more beneficial for removing dye pollutants from water. To this end, long-chain hydrophilic fluorinated groups have been reported to confer superhydrophilic surface properties [35], as well as play a key role in absorbing smaller dye molecules from water. A variety of hydrophilic synthetic material-based aerogels have been fabricated, including activated carbon [36], silica [37], fluorinated melamine sponge [38], and graphene sponge [39]. However, synthetic aerogels are disadvantageous in terms of biodegradability and costs. This drives the urgent need for economical and environmentally friendly aerogels, like those made from renewable sources (e.g., biomass waste). For example, large quantities of durian shells are discarded after consumption, leading to the requirement for waste treatment and resource waste. Durian shell waste, an inexpensive and widely available biomass, possesses a high content of lignin, cellulose, hemicellulose, and phenolic compounds, as well as amidogen, carboxyl, and hydroxyl functional groups, making it a promising material for fabricating sustainable porous adsorbents [40].

In this study, to effectively remove Rhodamine B (RhB) dye from aqueous solution, we explore the possibility of using durian shell waste as the raw material and via a straightforward modification process using long-chain sodium perfluoro butanoic acid (NAPFBA) and iron oxide particles to fabricate superhydrophilic aerogels with tunable characteristics. The prepared three-dimensional superhydrophilic aerogels were thoroughly characterized, then the effectiveness of RhB removal was examined under the influence of various factors, including initial dye concentration, adsorbent dosage, and solution pH. Density functional theory (DFT) was employed to assess the molecular-level binding interactions underlying the adsorption behavior. This study provides valuable insights for advancing the development of green adsorbents for the efficient removal of RhB contaminants from wastewater.

#### 2. Experimental

# 2.1. Materials

Durian shell waste was collected from a fruit store in Gothenburg, Sweden. Chitosan (95 % deacetylation; viscosity = 80–200 mPa  $\cdot$  s) was purchased from Nordic BioLabs. Sodium hydroxide (NaOH, Product No.

S5881), iron oxide (Fe $_3$ O $_4$ , Product No. 310069), silicon oil (5 mPa · s, Product No. 317667), Rhodamine B (RhB, Product No. R6626) dye, and acetic acid (Product No. A6283) were purchased from Sigma-Aldrich. Perfluorobutanoate was purchased from Fischer Scientific. All reagents were analytically pure and utilized without additional treatment.

#### 2.2. Aerogel preparation and surface functionalization

In this study, durian shell was used as the precursor for making the superhydrophilic/oleophobic aerogels. Fig. 1 overviews the preparation procedure of the aerogel. Firstly, the inner layer of the waste durian shell was peeled off, cut into smaller pieces (approximate dimensions of 2 cm by 3 cm by 1 cm), and washed using ethanol. For the hydrotreatment step, they were placed in a Teflon-lined autoclave (KH200, Germany) for 12 h at 200  $^{\circ}$ C, then washed using deionized water to remove water-soluble impurities. Subsequently, the hydrothermally pretreated samples were freeze-dried for 24 h at  $-80~^{\circ}$ C (Triad freeze dryer, USA), resulting in the aerogels with slightly reduced volumes but still retaining the original cuboid shapes.

To prepare the 0.10 mol/L sodium perfluorobutanoate (NaPFBA) solution, 1.07 g of perfluorobutanoic acid (PFBA) was dissolved in 50 mL of distilled under continuous stirring, then 0.2 g of sodium hydroxide (NaOH) was gradually added. To create a stable chitosan suspension, 0.05 g of chitosan was dissolved in 25 mL of 1 % (v/v) acetic acid solution, which was prepared by diluting 0.25 mL of acetic acid in distilled water. Then, 5 mL of the prepared NaPFBA solution was added to the chitosan suspension under continuous stirring, after which 0.1 g of Fe<sub>3</sub>O<sub>4</sub> particles were dispersed using an ultrasonic bath for at least 15 minutes to ensure uniform distribution and avoid aggregation [38]. The prepared aerogels were repeatedly immersed and squeezed in this formulation, then dried in a heated oven at 80 °C for 48 h. The resulting aerogel had an exceptionally low density of just 0.02 g/cm³, allowing it to be easily be supported on a Lunaria annua flower, as depicted in Fig. 1.

#### 2.3. Materials characterizations

The surface morphology of the aerogel was analyzed using a scanning electron microscope (SEM, JEOL JSM-7800F Prime, Japan). Before observation, the sample was coated with gold for 5 min using a sputtering coater (Desk-II; Denton Vacuum, Japan). To identify the chemical functional groups, present on the samples, a Nicolet Impact 420 FTIR spectrometer (Nicolet, USA) equipped with an attenuated total reflection (ATR) system was used to collect spectra in the range of 600–4000 cm $^{-1}$ . The crystalline structures of the samples were characterized via powder X-ray diffraction (XRD; Bruker AXS D8 Discover) using Cu K $\alpha$  radiation ( $\lambda=1.5406$  Å) with a scanning rate of  $2^{\circ}$ /min over a  $2\theta$  range. The crystallinity of the samples was evaluated using the Segal method, which is an empirical approach to determine the Crystallinity Index (CI) with the following equation [41]:

$$CI\ (\%) = \frac{I_{002} - I_{am}}{I_{002}} \times 100 \tag{1}$$

where  $I_{002}$  is the maximum intensity of the crystalline peak at approximately  $2\theta\approx 22^\circ$ , and  $I_{am}$  is the minimum intensity at approximately  $2\theta\approx 18^\circ$ , representing the amorphous region.

Additionally, the crystalline-to-amorphous (C:A) ratio was estimated using the CI values to quantify the relative amount of crystalline and amorphous regions in the samples. The C:A ratio was calculated as follows:

$$C: A = \frac{CI}{100 - CI} \tag{2}$$

The XPS measurements were conducted using a PHI 5700 spectrometer (Japan) with Al K $\alpha$  radiation (1486.6 eV) as the source. XPS

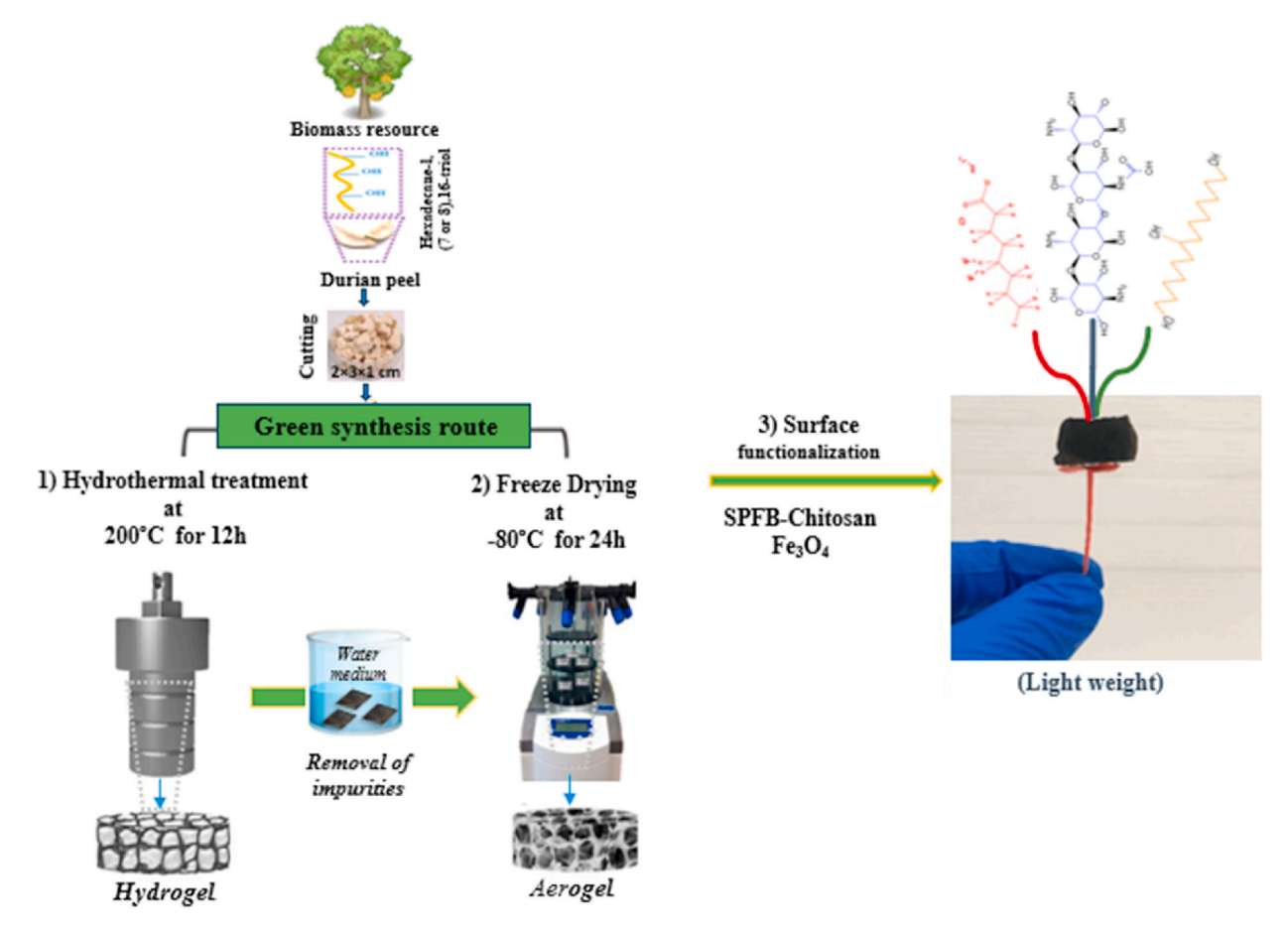


Fig. 1. Overview of preparation procedure of durian shell waste - derived, surface-modified aerogel.

Peak 4.1 software was utilized for peak-fitting and data analysis of the XPS spectra. The oil and water contact angles were measured at ambient conditions using a contact angle goniometer (KSVCM20, Finland); 3  $\mu L$  droplets of oil and water were analyzed. To analyze the textural characteristics, nitrogen adsorption—desorption experiments were conducted using a surface area analyzer (Quanta Chrome, USA) at 77 K. A 3000D digital camera (Nikon, Japan) was used to capture all the optical images.

#### 2.4. Adsorption of dye-rich water from oil medium

The phenomenon of selective absorption of RhB-rich (5 ppm) water by the durian shell waste – derived, surface-modified aerogel in a silicon oil medium is presented in Fig. 2 and Supplementary Video S1. The absorption capacity was determined by measuring the change in mass at room temperature after immersing an aerogel sample in the RhB-rich water until saturation was reached. The mass-based absorbency  $Q_{\rm w}$  was calculated using Equation (3):

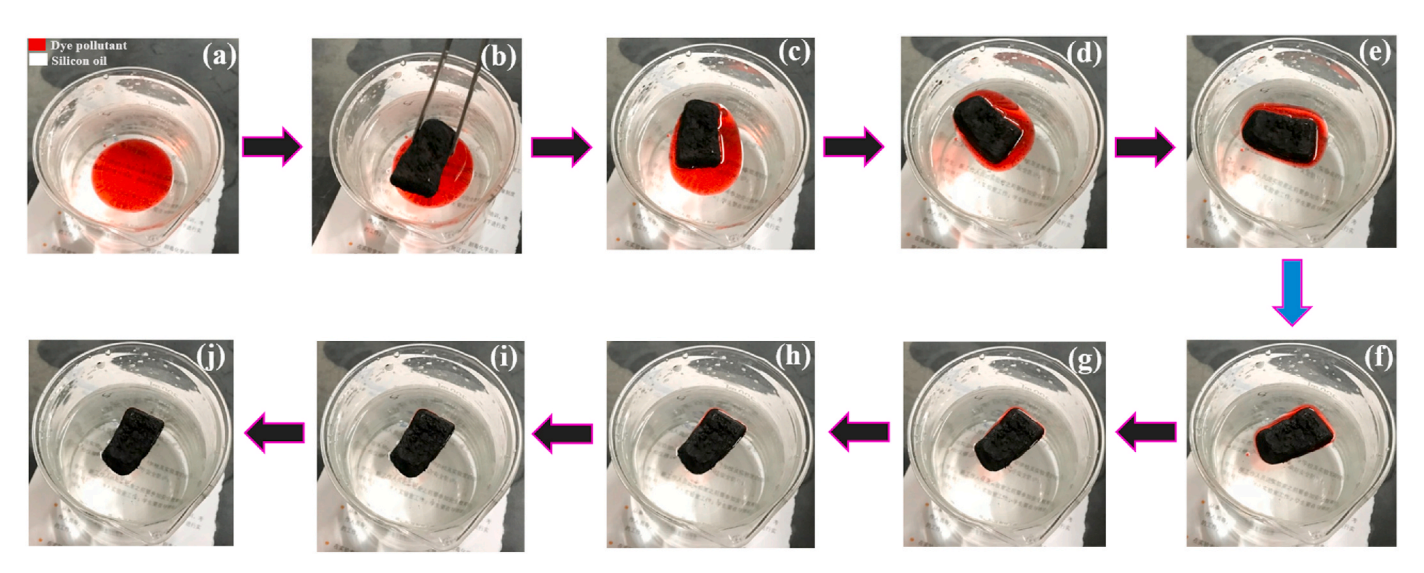


Fig. 2. Removal of RhB-rich water from the silicon oil medium.

$$Q_{w} = (m_{s} - m_{o}) / m_{o}$$
(3)

where  $m_s$  and  $m_0$  represent the masses of the aerogel before and after saturation.

#### 2.5. RhB dye adsorption experiments

To investigate the adsorption behavior, a typical dye, RhB ( $\lambda_{max}=554$  nm), was used. For each test, 0.39 g of aerogel was added to 50 mL of 15 mg/L RhB solution at 25 °C. Samples were collected using a syringe and filtered through with a 0.45µm Whatman® filter paper before RhB concentration was determined using a UV–vis spectrophotometer. The absorption capacity ( $Q_t$ ; mg/g) and removal efficiency (RE; %) were calculated using Equations (4) and (5):

$$Q_{t} = \frac{(C_{o} - C_{t})V}{m} \tag{4}$$

RE (%) = 
$$\frac{C_o - C_t}{C_o} \times 100$$
 (5)

where  $C_0$  and  $C_t$  (mg/L) are the concentrations of the solution at 0 and t (min), respectively, V (L) is the volume of the dye solution, and m (g) is the mass of the aerogel.

To further understand the adsorption behavior, adsorption kinetics were examined using the pseudo-first-order and pseudo-second-order models, as described by Equations (6) and (7), respectively [42]:

$$ln(Q_e - Q_t) = ln Q_e - (k_1 t) / 2.303$$
(6)

$$\frac{t}{Q_{t}} = \frac{1}{k_{2}Q_{e}^{2}} + \frac{t}{Q_{e}} \tag{7}$$

where  $k_1$  (/min) and  $k_2$  (g/mg min) are the kinetic rate constants of respectively the pseudo-first-order and pseudo-second-order models,  $Q_e$  (mg/g) and  $Q_t$  (mg/g) are the adsorption amounts respectively at equilibrium and at t (min). For the pseudo-first-order model, parameters  $k_1$  and  $Q_e$  were determined using the slope and intercept of the linear plot of log  $(Q_e$ -  $Q_t)$  versus time (t). For the pseudo-second-order model,  $Q_e$  and  $k_2$  were obtained from the linear relationship between  $t/Q_t$  and t.

Furthermore, to understand the adsorption mechanisms, isotherm data were collected from adsorption experiments over a range of initial RhB concentrations of 5–20 mg/L, and fitted to Langmuir and Freundlich models, as defined by Equations (8) and (9), respectively:

$$\frac{C_e}{Q_e} = \frac{1}{Q_m k_L} + C_e / Q_m \tag{8}$$

$$ln Q_e = ln k_F + \frac{1}{n} ln C_e$$
 (9)

where  $C_e$  (mg/L) is the concentration of the solution when the adsorption reaches equilibrium,  $Q_e$  (mg/g) is the amount of dye adsorbed at equilibrium,  $Q_m$  (mg/g) is the theoretical saturation capacity,  $k_L$  (L/mg) represents the Langmuir characteristic constant, and  $k_F$  (mg/g) and n are Freundlich characteristic constants, which relates to adsorption capacity and intensity, respectively.

## 2.6. Reusability

To determine the potential for repeated use, post-adsorption aerogel was washed with deionized water for multiple times at room temperature followed by freeze-drying at -60 °C, then reused for adsorption. The absorption capacity was examined through nine successive adsorption-regeneration cycles.

#### 2.7. Density functional theory (DFT)

Computational simulations were performed by the Vienna ab initio simulation package (VASP) with the projector augmented wave pseudopotentials (PAW) to describe the interaction between atomic cores and valence electrons with density functional theory (DFT) [43-45]. The Perdew-Burke-Ernzerhof (PBE) function within the generalized gradient approximation (GGA) was used to implement DFT calculations [46]. All calculations were spin-polarized. OGCOOH and OGOH slab models were employed to simulate the surface properties. The vacuum layer was set around 15 Å in the z-direction to avoid interaction between planes. The DFT-D3 method was employed for the consideration of van der Waals interaction. An energy cutoff for the plane wave basis expansion was set to 450 eV, and the force on each atom less than 0.03 eV/Å was set for the convergence criterion of geometry relaxation. The k-points in the Brillouin zone were sampled by a  $2\times2\times1$  grid [47]. The electronic energy was considered self-consistent with the energy change less than  $10^{-5}$  eV. VASPsol solvation was used to simulate the solvent effect in the experimental environment [48].

The adsorption energy (Eads) of adsorbate RhB was calculated using

$$E_{ads} = E_{RhB/surf} - E_{surf} - E_{RhB(g)}$$
 (10)

where  $E_{\rm RhB/surf}$ ,  $E_{\rm surf}$ , and  $E_{\rm RhB(g)}$  are the energy of RhB adsorption on the surface, the energy of a clean surface, and the energy of isolated RhB molecules in a cubic periodic box, respectively.

All geometry optimizations, including the implicit solvent effect with SMD, were implemented by the Gaussian package, and the harmonic frequency calculations were carried out to verify that all structures have no imaginary frequency [49]. The highest occupied molecular orbital (HOMO) and lowest unoccupied molecular orbital (LUMO) maps of different pollutants were rendered by using Visual Molecular Dynamics (VMD) software based on the files exported from Multifn 3.7 (dev) code with 0.02 isovalue [50,51].

#### 3. Results and discussion

# 3.1. Characterization of aerogels

The surface morphologies of the raw durian shell and the durian shell–derived, surface-modified aerogel are depicted in the SEM images in Fig. 3. Compared to the raw durian shell (Fig. 3(a)), the aerogel (Fig. 3 (c)) exhibited significantly greater surface porosity due to the hydrothermal synthesis procedure. Fig. 3(c) further shows the surface morphology of the aerogel at a greater magnification, indicating 3D, irregular, interconnected porous structures. These pores markedly enhance the surface area available for surface modification with NaPFBA–Fe<sub>3</sub>O<sub>4</sub>, thus augmenting the aerogel's capacity for adsorption.

Nitrogen adsorption-desorption tests were conducted to investigate the surface area and porosity of the aerogel. Fig. 4(a) shows the  $\rm N_2$  adsorption-desorption isotherm, indicating a clear hysteresis loop within the relative pressure range ( $P/P_0$ ) of 0.01–1.0. The observed adsorption isotherm follows a Langmuir Type IV pattern with an H3 hysteresis loop [52]. Fig. 4(b) shows the pore size distribution analyzed using the Barrett-Joyner-Halenda (BJH) method. The pores were in the 2–50 nm range (i.e., mesopores), with an average pore diameter of 6.14 nm. Furthermore, BET results indicated a high specific surface area of 116.2 m²/g and a pore volume of 0.0065 cm³/g.nm. The mesoporous structure and the high specific area of the aerogels are advantageous for dve adsorption.

To determine the crystallinity and identify the phases of the durian shell – derived, surface-modified aerogels, XRD analysis was performed. Fig. 5(a) shows that the aerogel exhibits peaks corresponding to NaPFBA, Chitosan and  $Fe_3O_4$ , which are absent in the raw durian shell, thereby affirming successful deposition of the NaPFBA-chitosan- $Fe_3O_4$  particles onto the surface of the aerogels [53,54]. The XRD spectra

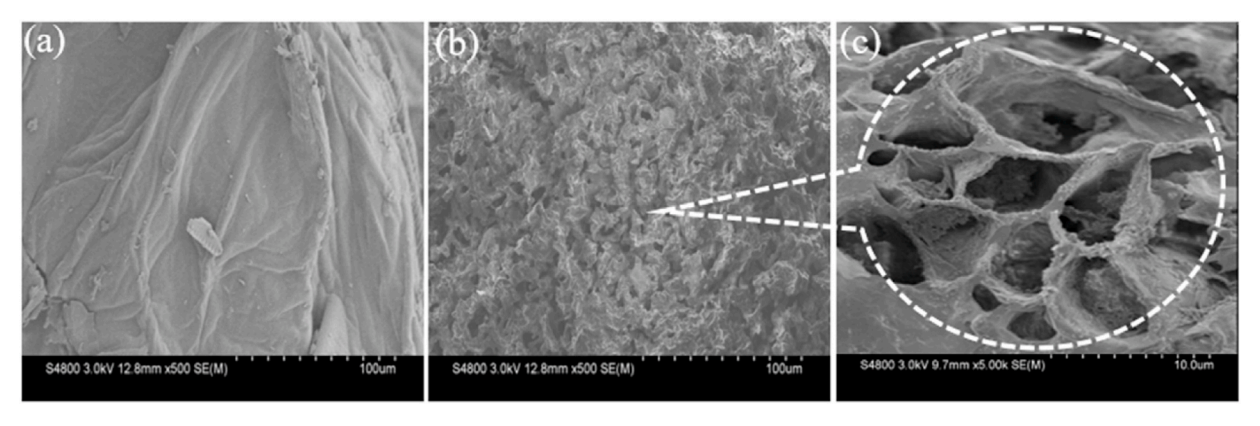


Fig. 3. SEM images of (a) raw durian shell, (b) durian shell – derived, surface-modified aerogel, and (c) zoomed in image of (b) to show the 3D interconnected pore structures.

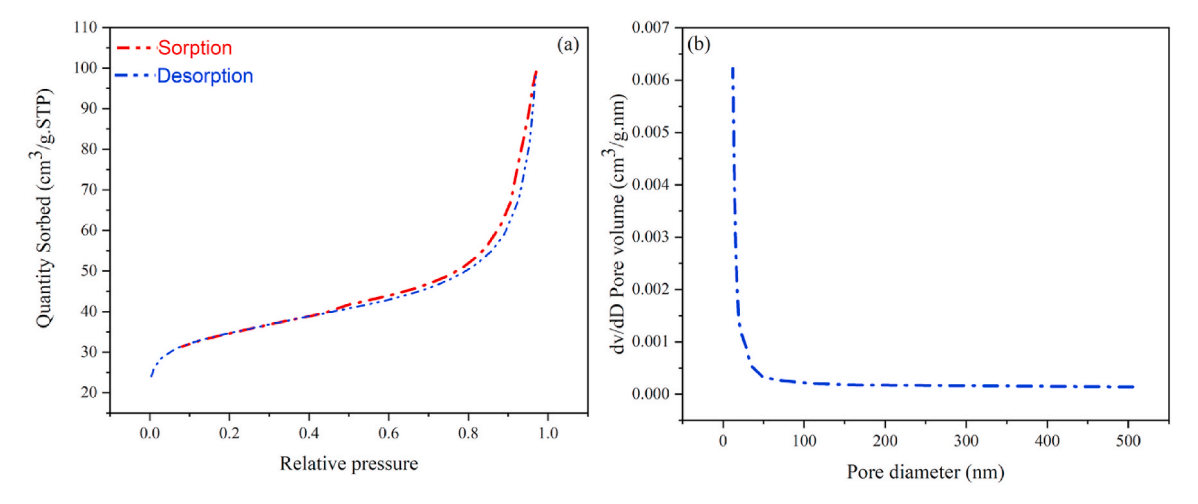


Fig. 4. (a)  $N_2$  adsorption-desorption isotherm, and (b) pore size distribution curve of the durian shell – derived, surface-modified aerogel.

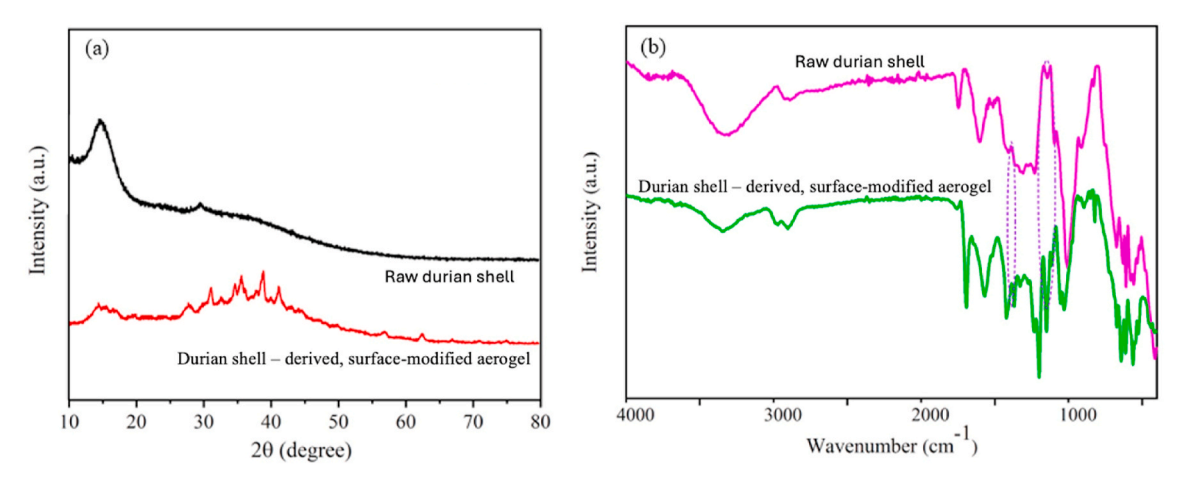


Fig. 5. (a) XRD and (b) FTIR spectra of the raw durian shell and durian shell – derived, surface-modified aerogel.

reveal the more crystalline structure of the raw durian shell, with a pronounced peak at around  $2\theta\approx12^\circ\text{--}20^\circ\text{.}$  In contrast, the surface-modified aerogel exhibited a broader, less intense peaks, indicating a more amorphous structure. Quantitatively, the Crystallinity Index (CI) of the raw durian shell was 27.03 %, while that of the modified aerogel decreased to 9.66 %, reflecting a significant reduction in crystallinity upon the hydrothermal and freeze-drying process. The crystalline-to-amorphous (C:A) ratio, derived from the CI values, further

confirmed the structural changes. The raw durian shell and surface-modified aerogel had C:A ratios of 0.37 and 0.11, respectively, indicating a marked decrease in crystallinity after modification.

Furthermore, the surface functional groups were characterized using the FTIR, as presented in Fig. 5(b). The FTIR spectrum of the raw durian shell exhibits characteristic peaks at 3480, 1548, 1261, and 810 cm $^{-1}$ , corresponding to the stretching vibrations of C=C/C-N, -N-H, -C-O-, and triazine ring bending, respectively [55]. Additionally, the peak

observed at 2895 cm $^{-1}$  corresponds to the -C-H stretching vibration, while the bands at 1480 and 1339 cm $^{-1}$  are attributed to -C-H bending vibrations. Regarding the durian shell–derived, surface-modified aerogel, the FTIR spectrum reveals a distinct new peak at 1665 cm $^{-1}$ , indicating the presence of >C--O stretching vibration. The emergence of new distinctive bands in the spectral region of 1150–1198 cm $^{-1}$  is attributed to -C-F- groups, affirming the successful surface deposition of NaPFBA -chitosan-Fe<sub>3</sub>O<sub>4</sub> onto the aerogels [55]. The oleophobicity of the aerogel is attributed to the reduced surface free energy induced by -C-F bonds, as well as an increased concentration of >C--O functional groups [54,56,57].

Fig. 6(a) displays the XPS survey spectrum of the durian shell derived, surface-modified aerogel, indicating peaks characteristic of the elements Fe, F, N, O, and C. The significantly higher fluorine amounts (39.55 atomic %) compared to other elements provide strong evidence of the successful deposition of NaPFBA onto the aerogel surface. This observation was further confirmed by the presence of aliphatic -F-Cbonds, as reflected in the FTIR spectrum in Fig. 5(b). Chemical modifications with respect to the O/C and F/C ratios enabled tailoring of the wetting characteristics of the aerogels [58]. The high-resolution C1s spectrum of the aerogels presented in Fig 6(a) shows well-defined peaks for the CO-, -CH<sub>2</sub>-, -CO<sub>3</sub>-, -CO-, -CO<sub>3</sub>-, and -CF<sub>2</sub>- groups, corresponding to binding energies of 294, 292, 290, 288, 286, and 285 eV respectively. Additionally, the full width at half minimum (FWHM) of these peaks was measured to be approximately 1.7 [59]. After applying the NaPFBA coating, the distribution of functional oleophobic CF<sub>2</sub>- and CF<sub>3</sub>- groups amounted to 30.11 % and 2.70 %, respectively, signifying the presence of low surface energy species. Nonetheless, the raw durian shell contributed to 22.34 % COO- and 4.37 % CO- groups, denoting polar functionalities and hydrophilic characteristics. The excellent dye adsorption behavior was tailored surface-modification of the aerogels with hydrophilic and oleophobic groups via intercalated pathways, while the induced alignment of hydrophilic and oleophobic groups confer a 3D capillary effect. The durian shell-derived, surface-modified aerogel can thus effectively block the permeation of non-polar liquid droplets via oleophobic fluorinated groups, giving excellent superhydrophilic/oleophobic characteristics. Moreover, the introduction of fluorination and the attachment of Fe<sub>3</sub>O<sub>4</sub> particles were to significantly enhance the permeation of dye molecules through the aerogel.

As presented in Fig. 7, chitosan effectively adheres to 1, (7 or 8),16-hexadecanetriol derivatives by forming ionic or covalent bonds on the raw durian shell surface. Subsequently, the long chains of NaPFBA and

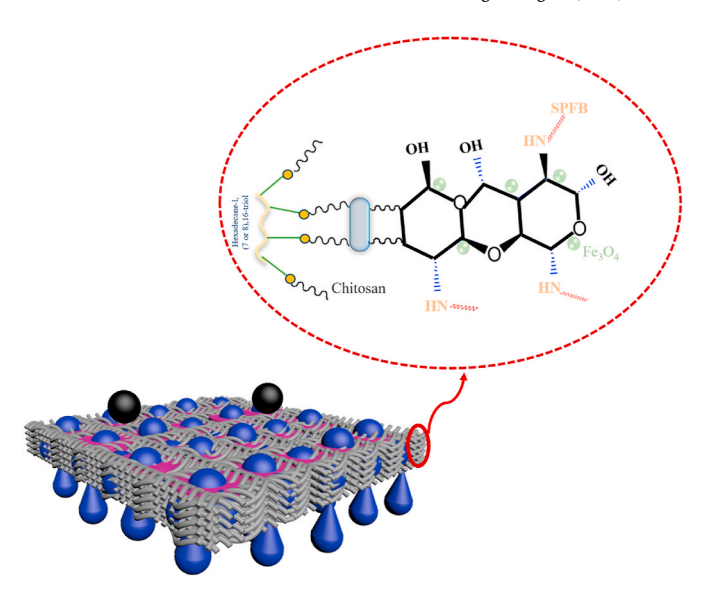
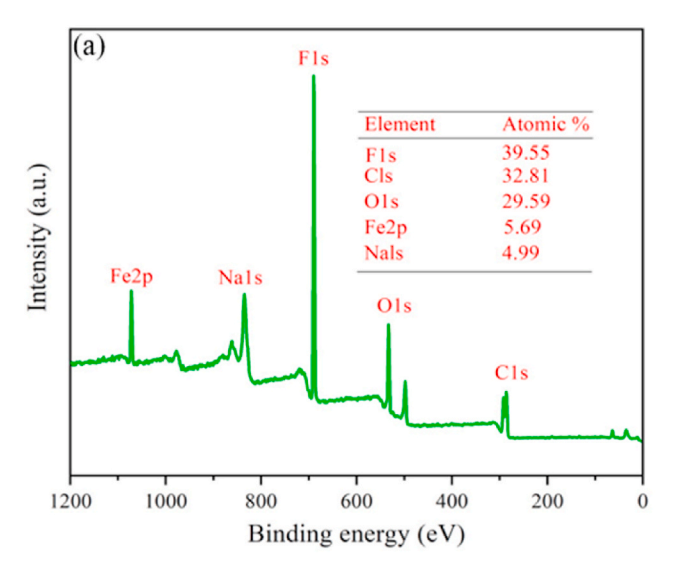


Fig. 7. Surface modifications of the durian shell – derived, surface-modified aerogel to enhance adsorption.

 $Fe_3O_4$  particles, exhibiting superhydrophilic/oleophobic properties, likely attaches to the poly-aromatic cyclic framework of chitosan via ionic or covalent bonds [60]. Therefore, the results provide compelling evidence that the significant porosity of the aerogels, combined with the superhydrophilic/oleophobic design of NaPFBA, chitosan and  $Fe_3O_4$  on the surface, can synergistically contribute to remarkable adsorption of dyes by these durian shell – derived, surface-modified aerogels.

The physical properties of the durian shell – derived, surface-modified aerogels were investigated through a series of analytical tests. Despite the exceptionally low density of  $0.02\,\mathrm{g/cm^3}$  that allows the aerogels to be supportable by flower (Lunaria annua) petals, the mechanical properties are outstanding. As presented in Fig. 8(a) and Supplementary Video S2, a  $0.02\,\mathrm{g}$  aerogel withstood a 1 kg weight without any observable deformation. Additionally, the superior superhydrophilic/oleophobic properties of B-MA are illustrated in Fig. 8(b) and Supplementary Video S3, where the aerogel simply floats on the oil surface due to the unfavorable interactions. Fig. 8(c) and Supplementary Video S4 further show that, when an aerogel sample was intentionally immersed in the oil and subjected to a mechanical force through a tweezer, a significant number of air bubbles formed on the aerogel



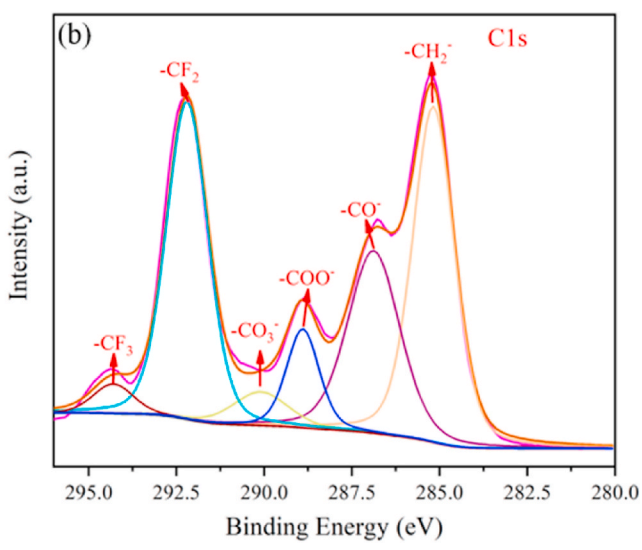


Fig. 6. (a) XPS survey analysis and (b) high-resolution C1s fitted spectra of the durian shell - derived, surface-modified aerogel.

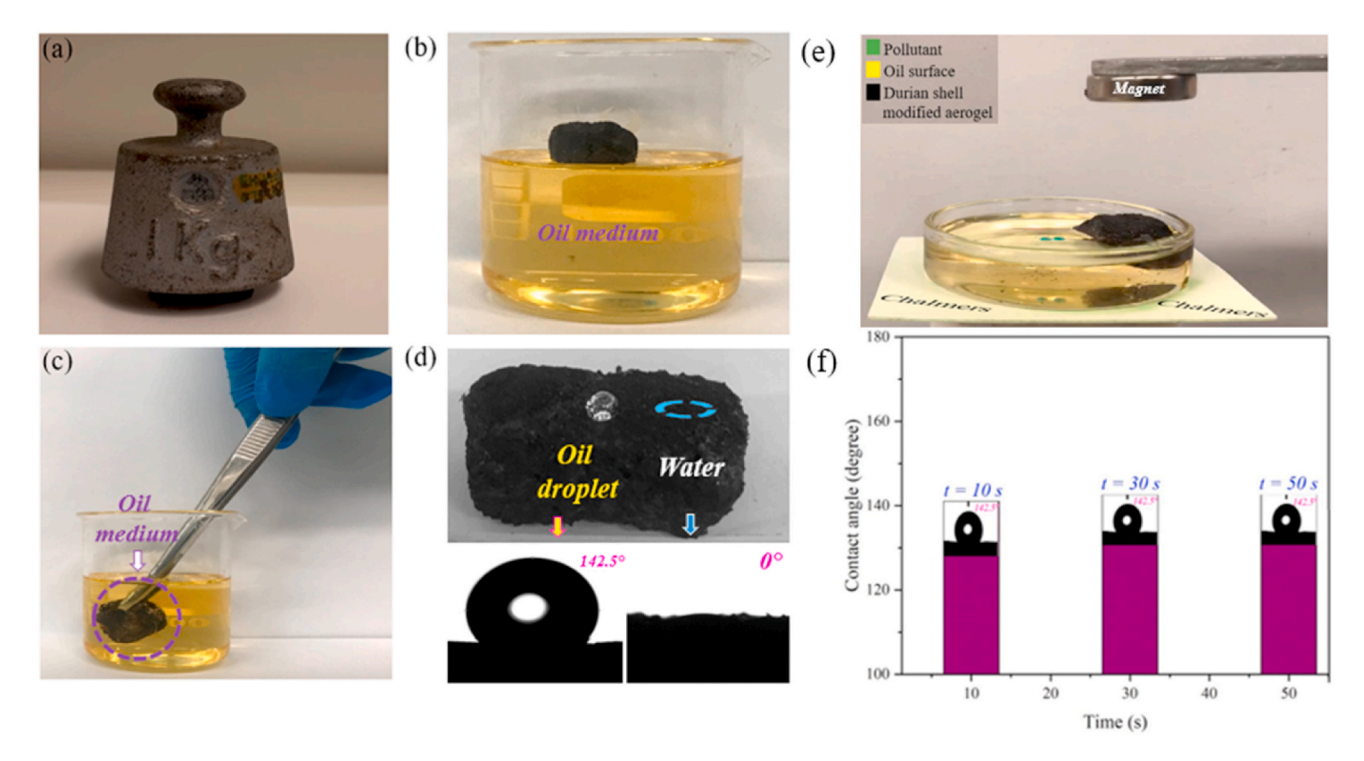


Fig. 8. Physical characteristics of durian shell – derived, surface-modified aerogel: (a) withstood a 1 kg weight without mechanical deformation; (b) floated on oil medium; (c) formation of air bubbles when immersed and slight mechanical force applied; (d) oil and water contact angles; (e) directional mobility induced by magnet; and (f) oil contact angles over time.

surface, evidencing its superhydrophilic/oleophobic property. The oil and water contact angles were quantified as 142.5° and 0°, respectively, with the oil contact angle demonstrated to remain constant over a minute (Fig. 8(f)). As shown in Fig. 8(d) and Supplementary Video S5, the oil droplet remained as a droplet, while the water droplet dispersed onto the aerogel surface. The wettability of the aerogels in this study is superior to that of previously reported biomass-derived porous aerogels [61,62], though pales in comparison to aerogels made from synthetic materials [63-65]. The differences in contact angles are likely a result of distinct surface energy levels and geometric compositional arrangements [65]. Furthermore, the presence of iron oxide on the aerogel surface conferred the ability to control the directional mobility of the aerogel by using a magnet, as shown in Fig. 8(e) and Supplementary Video S6. This allows for the possibility of directing the aerogels specifically to the contaminated regions in wastewater treatment applications.

#### 3.2. Dye adsorption

The dye separation capability of the durian shell waste – derived, surface-modified aerogels was assessed. Fig. 9 shows the redness of the RhB-rich (15 mg/L) solution was significantly reduced after adsorption by the aerogels. Under a high-resolution optical microscope, Fig. 9(a) shows a dense distribution of dye particles in the RhB-rich solution, while Fig. 9(b) shows that the dye particles have largely disappeared after adsorption by the aerogels. The adsorption capacity (Qt) and removal efficiency (RE) for the initial RhB concentration of 15 mg/L were calculated to evaluate the performance of the aerogels. The adsorption capacity, which represents the amount of dye adsorbed per gram of aerogel, was observed to increase with time, reaching a maximum equilibrium value of 14.42 mg/g at 60 minutes. The removal efficiency of the dye was also significant at 96.1 %. These results highlight the superior adsorption performance of the aerogels. The adsorption performance of the modified aerogel was further analyzed using both kinetic (Fig. 10(a) and (b)) and isotherm (Fig. 10(c) and (d)) models to quantify its efficacy in removing RhB from water. The results

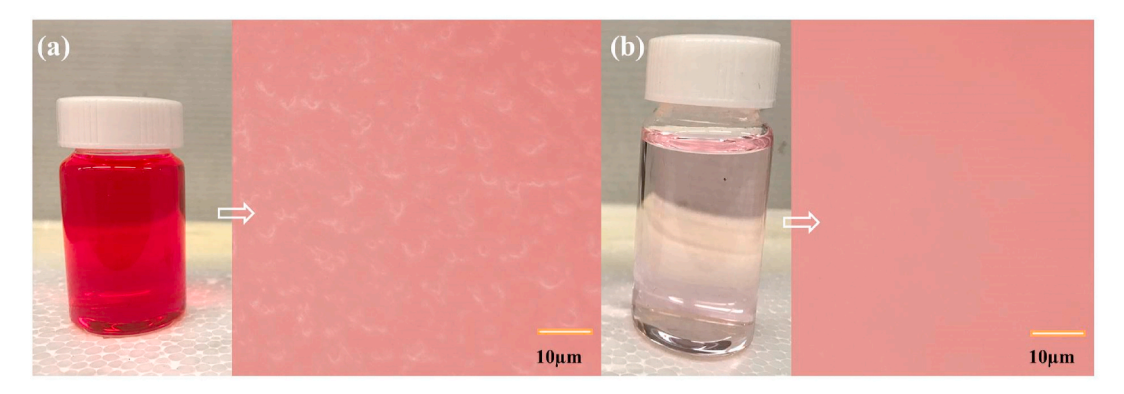


Fig. 9. Optical images: (a) before adsorption and (b) after adsorption by durian shell waste - derived, surface-modified aerogels.

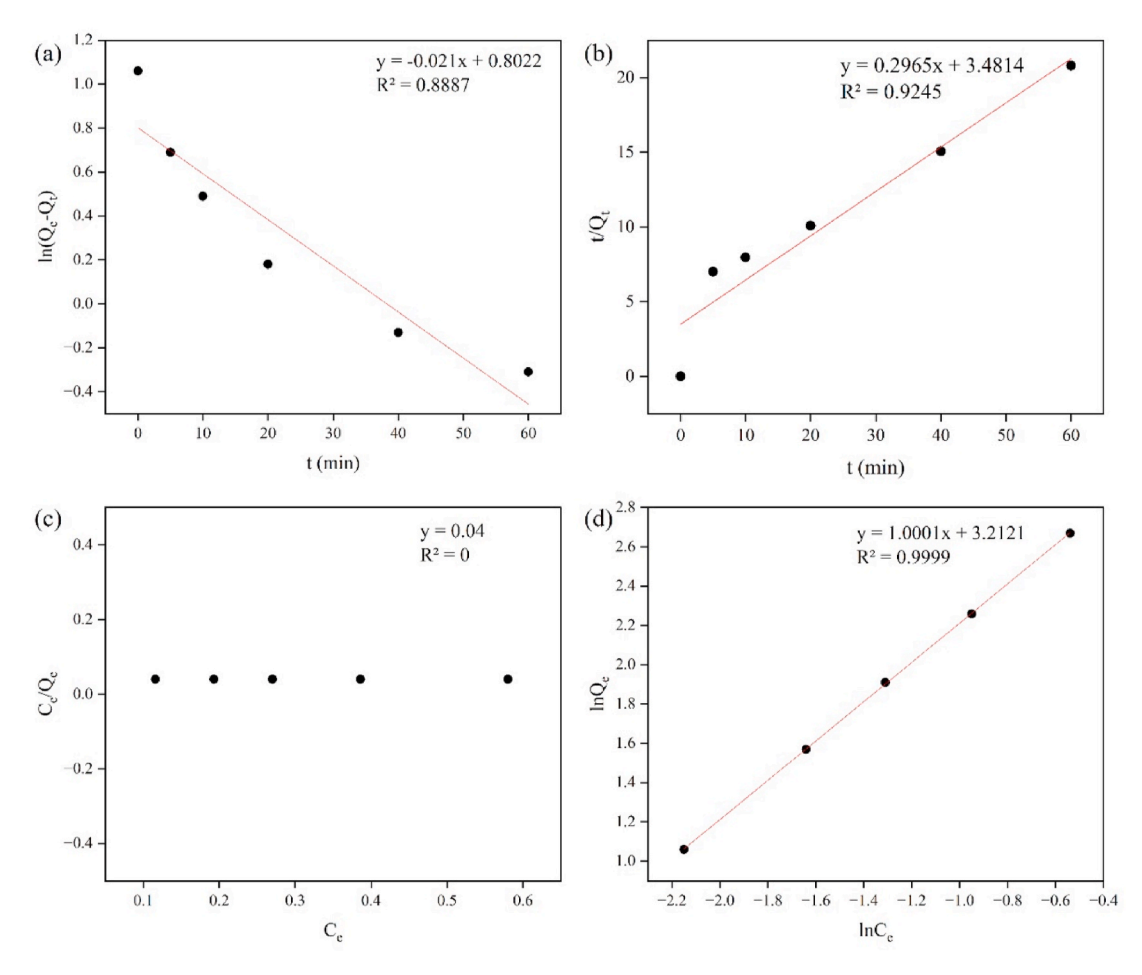


Fig. 10. Modelling dye adsorption by durian shell waste – derived, surface-modified aerogels: (a) pseudo-first-order kinetic model; (b) pseudo-second-order kinetic model; (c) Langmuir isotherm; and (d) Freundlich isotherm.

from the kinetic and isotherm studies are summarized in Tables 1 and 2, respectively.

The kinetics of adsorption was assessed using pseudo-first-order and pseudo-second-order models (Fig. 10(a) and (b)). The pseudo-first-order model, which assumes that the rate of adsorption is proportional to the number of unoccupied sites, gives a moderate fit with an  $R^2$  value of 0.8887. The rate constant ( $K_1=0.021$ ) and equilibrium adsorption capacity ( $q_e=2.884~\text{mg/g}$ ) indicate a partial contribution of physical adsorption. However, the pseudo-second-order model demonstrates a better correlation with an  $R^2$  value of 0.9245, suggesting that adsorption is predominantly governed by chemical interactions between the adsorbent and adsorbate, rather than being limited by physical diffusion. The rate constant ( $K_2=0.2965~\text{min}^{-1}$ ) and the equilibrium adsorption capacity ( $q_e=2.884~\text{mg/g}$ ) reveal that chemisorption plays a dominant role in the adsorption. These findings suggest that the adsorption of dye molecules onto the aerogel surface is primarily governed by adsorbent-adsorbate chemical interactions.

The equilibrium adsorption behavior was analyzed using the Langmuir and Freundlich isotherm models. The Langmuir model, which assumes monolayer adsorption onto a homogeneous surface, shows a poor fit with an  $\mathbb{R}^2$  value of 0.00, indicating that the adsorption mechanism of

**Table 1**Pseudo-first-order and pseudo-second-order model parameters, calculated through data-fitting.

Kinetic Model	q <sub>e</sub> (mg/g)	K <sub>1</sub> or K <sub>2</sub> (1/min)	$\mathbb{R}^2$
Pseudo-First-Order Pseudo-Second-Order	$\begin{array}{c} 2.884 \pm 0.05 \\ 2.884 \pm 0.05 \end{array}$	$\begin{split} K_1 &= 0.021 \pm 0.001 \\ K_2 &= 0.2965 \pm 0.004 \end{split}$	0.8887 0.9245

**Table 2**Adsorption isotherm constants for the Langmuir and Freundlich models, obtained through data-fitting.

lsotherm Model	$q_{max}$ or $K_F$ (mg/g)	$K_L$ (L/mg) or n	$R^2$
Langmuir Freundlich	$\begin{aligned} q_{max} &= 0.04 \\ K_F &= 24.85 \pm 0.3 \end{aligned} \label{eq:max}$	$\stackrel{-}{n}=1.0\pm0.01$	0.00 0.9999

the aerogel is not via monolayer. In contrast, the Freundlich model, which accounts for multilayer adsorption on heterogeneous surfaces, exhibits an excellent fit with an  $R^2$  value of 0.9999. The Freundlich constant ( $K_F=24.85$ ) suggests a high adsorption capacity, while the adsorption intensity constant (n = 1.0) indicates a favorable and relatively uniform adsorption process, across different energy sites. These results confirm the heterogeneous nature of the adsorption sites on the aerogels and the strong affinity for dye molecules. Furthermore, BET results (Fig. S1 and Table S1) after the adsorption tests indicate negligible changes in pore diameter, pore volume and surface area, reflecting the stability of the porous structure during adsorption.

Overall, the adsorption results demonstrate that the durian shell waste–derived, surface-modified aerogels exhibit exceptional performance in RhB dye removal, driven by chemisorption mechanisms and heterogeneous surface properties (based on adherence to the Freundlich isotherm and pseudo-second-order kinetic model). This underscores the potential of the aerogels as efficient adsorbents for environmental remediation applications.

#### 3.3. Reusability

For sustainable applications, the reusability of the adsorbents is vital. Fig. 11(a) shows the adsorption capacities of RhB by the aerogels over nine adsorption-regeneration cycles, indicating only slight decreases with each reuse and the removal rate remaining at above 96 % at the end of nine cycles. Fig. 11(b) and (c) show the images of the aerogels after adsorption and after regeneration, indicating the porous structures remain intact. The high reusability performance is due to retention of the integrity of the porous structure and chemical interaction sites on the aerogels over repeated use. The excellent reusability makes such aerogels promising for practical implementation in dye removal applications.

#### 3.4. DFT insights

To explore the adsorption mechanism, density functional theory (DFT) calculations of the interactions between the hydrophilic/oleophobic molecular sites of the aerogels and RhB molecules were conducted. Fig. 12 depicts the frontier molecular orbitals - highest occupied molecular orbital (HOMO) and lowest unoccupied molecular orbital (LUMO) - and the optimized geometries of the active sites and RhB molecule, while Table 3 lists the corresponding energies. The orbitals highlight the functional regions responsible for donor-acceptor interactions in each molecule. The HOMO distribution is primarily localized around oxygen-containing functional groups, such as hydroxyl, methoxy, carboxyl, and aromatic rings. The lone pairs and  $\pi$ -electrons within these regions act as electron-donating sites, contributing to the filling of vacant orbitals in RhB dye molecules. On the other hand, the LUMO is predominantly distributed over residual carboxylic acid groups, highlighting their potential as charge acceptors from RhB. In RhB molecules, the HOMO is mainly concentrated around the chlorine atom, nitrogen atom, and aromatic benzene rings, whereas the LUMO is distributed around the sulfur atom, nitrogen heteroatom, and benzene rings, where delocalized  $\pi$ -electrons contribute to its electronic characteristics. The geometry of the aerogels combined with NaPFBA supports both HOMO and LUMO distributions, highlighting that the carboxyl group can act as both an electron donor and an acceptor. The surface of the aerogel is predominantly characterized by HOMO and LUMO distributions, with electron-donating characteristics attributed to benzene rings near hydroxyl and epoxy groups. Furthermore, the presence of electron-withdrawing groups significantly influences the positions of the HOMO and LUMO within the molecular structure.

DFT calculations reveal that the adsorption mechanism of RhB on the aerogel is primarily driven by electronic interactions between RhB and  $\,$ 

the active sites, namely, OGCOOH and OGOH. OGCOOH. The small HOMO-LUMO gap and strong adsorption energy (-2.225 eV) exhibited by OGCOOH gives the highest reactivity and adsorption capacity for RhB, making it the dominant active site for RhB removal. The relatively small energy gap of OGOH (0.0159 eV) also indicates significant reactivity, though its interaction with RhB is less exothermic (-1.825 eV) compared to OGCOOH, suggesting a weaker adsorption strength. In contrast, NaPFBA and chitosan, with larger energy gaps (2.8563 eV and 4.2125 eV, respectively), exhibit weaker electronic reactivity and adsorption potential, making them play less significant roles in RhB adsorption. These findings suggest that OGCOOH plays a crucial role in facilitating RhB removal from aqueous solutions by the aerogel, with OGOH also contributing, albeit to a lesser extent. These results provide valuable insights into the design of effective aerogel materials for organic pollutant removal based on the electronic properties of the active sites.

#### 4. Conclusion

This study presents a novel 3D porous carbon aerogel with superoleophobic/hydrophilic properties, derived from waste durian shells through a simple and green synthesis route. The aerogel was comprehensively characterized using a wide range of analytical techniques to assess its porosity, physicochemical properties, and functional performance. The Rhodamine B dye removal efficiency was experimentally investigated, while the underlying mechanisms were verified using DFT calculations. The exceptional high specific surface area and superhydrophilic/oleophobic properties conferred by surface functional groups of the aerogels enabled efficient removal of RhB from water. Moreover, DFT revealed that RhB exhibited a strong binding affinity to the aerogel surface via electrostatic interactions and hydrogen bonding. This study offers valuable insights for the strategic design and development of renewable, eco-friendly, cost-effective, and high-performance 3D porous adsorbent materials from biomass waste for environmental remediation.

#### 4.1. Future recommendations

- (1) For applicability to more complex wastewaters, examine the efficacy of such aerogels to remove a wider spectrum of contaminants, e.g., heavy metals, industrial dyes, pharmaceutical compounds, per- and polyfluoroalkyl substances.
- (2) For enhancing binding with specific contaminants, identify means to customize surface chemistry of aerogels for optimal interactions under different physiochemical conditions.

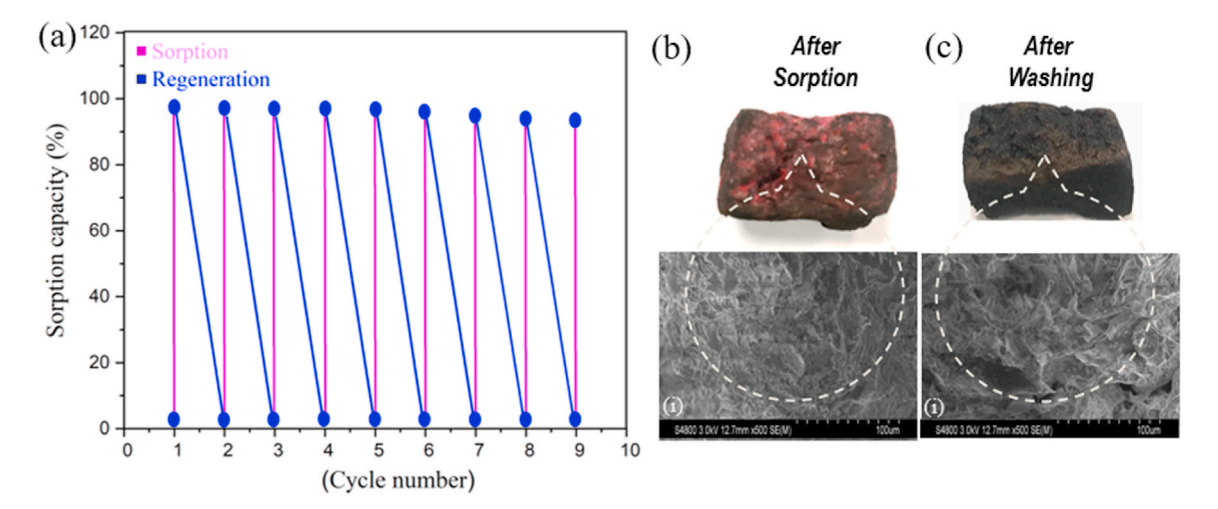


Fig. 11. Reusability of durian shell – derived, surface-modified aerogels: (a) adsorption capacity over nine adsorption-regeneration cycles; images of aerogels (b) after adsorption, and (c) after regeneration.

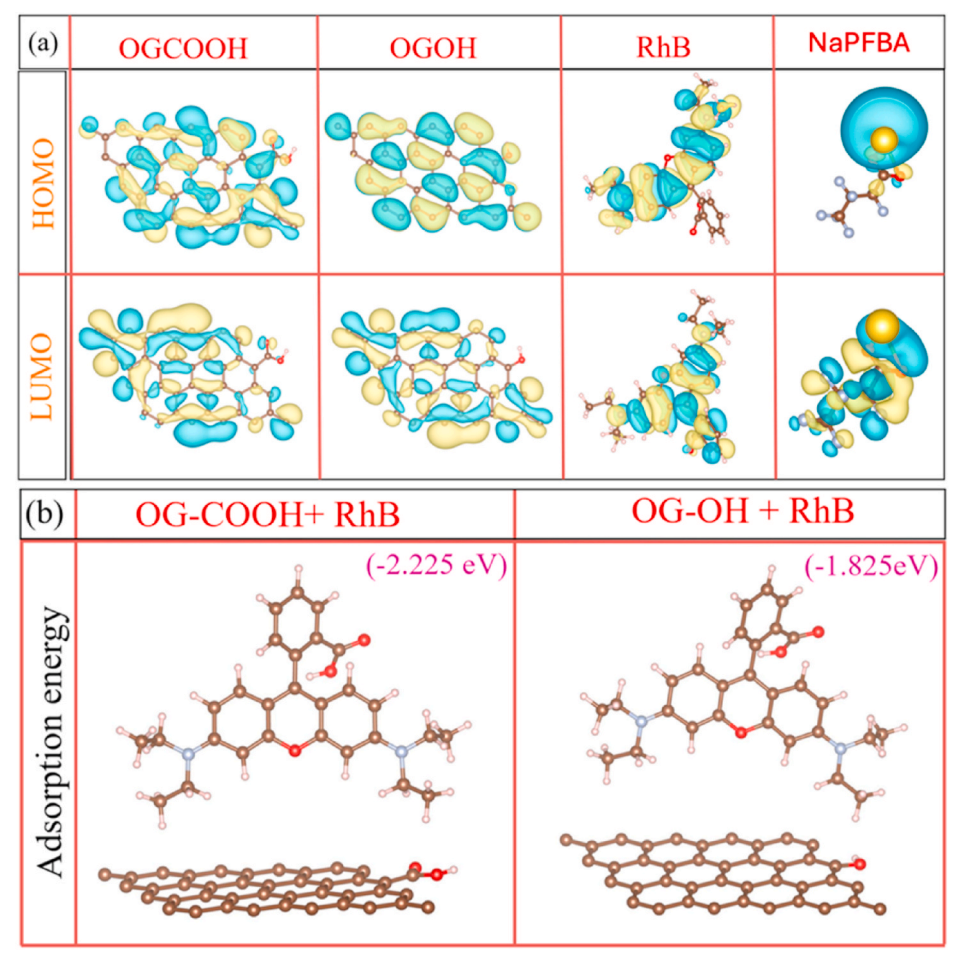


Fig. 12. (a) Frontier orbitals HOMO/LUMO and (b) optimized geometries of OGCOOH, OGOH, and RhB.

Table 3 The HOMO and LUMO energies (eV), energy gap ( $\Delta E_{\rm L-H})$  for SBPF, Chi, OGCOOH, OGOH and RhB.

Molecules	НОМО	LUMO	$\Delta EL_{-H}$
NaPFBA	-4.0313	-1.175	2.8563
chitosan	-5.3159	-1.1034	4.2125
OGCOOH	-5.5145	-5.3076	0.2069
OGOH	-5.4269	-5.411	0.0159
RhB	-5.3159	-1.1034	4.2125

- (3) For practical environmental remediation, assess the scalability and cost of the synthesis process, as well as long-term application in industrial-scale continuous-flow systems.
- (4) Evaluate potential for incorporation into composite materials and/or hybrid separation systems.

# CRediT authorship contribution statement

**Muhammad Imran:** Writing – original draft, Methodology, Investigation, Formal analysis, Data curation, Conceptualization. **Meilan Pan:** Methodology, Investigation, Formal analysis. **Ashraful Islam:** Investigation. **Jia Wei Chew:** Writing – review & editing, Supervision, Resources, Project administration, Investigation, Funding acquisition, Formal analysis, Data curation.

### Declaration of competing interest

The authors declare that they have no known competing financial

interests or personal relationships that could have appeared to influence the work reported in this paper.

#### Acknowledgment

This work was supported by Chalmers Gender Initiative for Excellence (Genie).

#### Appendix A. Supplementary data

Supplementary data to this article can be found online at https://doi.org/10.1016/j.cscee.2025.101238.

# Data availability

Data will be made available on request.

# References

- [1] H. Hosseini, A. Zirakjou, D.J. McClements, V. Goodarzi, W.H. Chen, Removal of methylene blue from wastewater using ternary nanocomposite aerogel systems: carboxymethyl cellulose grafted by polyacrylic acid and decorated with graphene oxide, J. Hazard. Mater. 421 (2022) 126752, https://doi.org/10.1016/j. jhazmat.2021.126752.
- [2] S. Wang, Y. Boyjoo, A. Choueib, Z.H. Zhu, Removal of dyes from aqueous solution using fly ash and red mud, Water Res. 39 (2005) 129–138, https://doi.org/ 10.1016/j.watres.2004.09.011.
- [3] X. Pan, S. Cheng, T. Su, G. Zuo, W. Zhao, X. Qi, W. Wei, W. Dong, Fenton-like catalyst Fe304@polydopamine-MnO2 for enhancing removal of methylene blue in wastewater, Colloids Surf. B Biointerfaces 181 (2019) 226–233, https://doi.org/ 10.1016/j.colsurfb.2019.05.048.

- [4] J. Pal, M.K. Deb, Efficient sorption of basic organic dyes from aqueous solution using green synthesized silver nanoparticles beads, J. Dispersion Sci. Technol. 34 (2013) 1193–1201, https://doi.org/10.1080/01932691.2012.739939.
- [5] L.F. Mottram, S. Forbes, B.D. Ackley, B.R. Peterson, Hydrophobic analogues of rhodamine B and rhodamine 101: potent fluorescent probes of mitochondria in living C. elegans, Beilstein J. Org. Chem. 8 (2012) 2156–2165, https://doi.org/ 10.3763/bios.8.243
- [6] G. Wang, J. Qi, S. Wang, Z. Wei, S. Li, J. Cui, W. Wei, Surface-bound humic acid increased rhodamine B adsorption on nanosized hydroxyapatite, J. Dispersion Sci. Technol. 38 (2017) 632–641, https://doi.org/10.1080/01932691.2016.1185729.
- [7] M. Kaushal, A. Tiwari, Removal of rhodamine-b from aqueous solution by adsorption onto crosslinked alginate beads, J. Dispersion Sci. Technol. 31 (2010) 438–441, https://doi.org/10.1080/01932690903210135.
- [8] V. da Silva Lacerda, J.B. López-Sotelo, A. Correa-Guimarães, S. Hernández-Navarro, M. Sánchez-Báscones, L.M. Navas-Gracia, P. Martín-Ramos, J. Martín-Gil, Rhodamine B removal with activated carbons obtained from lignocellulosic waste, J. Environ. Manag. 155 (2015) 67–76, https://doi.org/10.1016/j.ienvman.2015.03.007
- [9] V.K. Gupta, I. Ali, V.K. Saini, Removal of chlorophenols from wastewater using red mud: an aluminum industry waste, Environ. Sci. Technol. 38 (2004) 4012–4018, https://doi.org/10.1021/es049539d.
- [10] C. Baslak, G. Arslan, M. Kus, Y. Cengeloglu, Removal of Rhodamine B from water by using CdTeSe quantum dot-cellulose membrane composites, RSC Adv. 6 (2016) 18549–18557, https://doi.org/10.1039/c5ra23433f.
- [11] G. Jethave, U. Fegade, R. Rathod, J. Pawar, Dye pollutants removal from waste water using metal oxide nanoparticle embedded activated carbon: an immobilization study, J. Dispersion Sci. Technol. 40 (2019) 563–573, https://doi. org/10.1080/01932691.2018.1472016.
- [12] M.R.R. Kooh, M.K. Dahri, L.B.L. Lim, The removal of rhodamine B dye from aqueous solution using Casuarina equisetifolia needles as adsorbent, Cogent Environ. Sci. 2 (2016), https://doi.org/10.1080/23311843.2016.1140553.
- [13] N. Van Suc, D. Kim Chi, Removal of rhodamine B from aqueous solution via adsorption onto microwave-activated rice husk ash, J. Dispersion Sci. Technol. 38 (2017) 216–222, https://doi.org/10.1080/01932691.2016.1155153.
- [14] A. Sewnet, M. Abebe, P. Asaithambi, E. Alemayehu, Visible-light-driven g-C3N4/ TiO2 based heterojunction nanocomposites for photocatalytic degradation of organic dyes in wastewater: a review, Air Soil. Water Res. 15 (2022), https://doi. org/10.1177/11786221221117266.
- [15] D. Datta, Ö. Kerkez Kuyumcu, Ş.S. Bayazit, M. Abdel Salam, Adsorptive removal of malachite green and Rhodamine B dyes on Fe3O4/activated carbon composite, J. Dispersion Sci. Technol. 38 (2017) 1556–1562, https://doi.org/10.1080/ 01932691,2016.1262776.
- [16] S. Zhang, C. Yu, N. Liu, Y. Teng, C. Yin, Preparation of transparent anti-pollution cellulose carbamate regenerated cellulose membrane with high separation ability, Int. J. Biol. Macromol. 139 (2019) 332–341, https://doi.org/10.1016/j. iibiomac.2019.07.146.
- [17] X. Yue, H. Chen, T. Zhang, Z. Qiu, F. Qiu, D. Yang, Controllable fabrication of tendril-inspired hierarchical hybrid membrane for efficient recovering tellurium from photovoltaic waste, J. Clean. Prod. 230 (2019) 966–973, https://doi.org/ 10.1016/j.jclepro.2019.05.141
- [18] M. Imran, A. Islam, F. Ismail, P. Zhang, M. Basharat, M. Ikram, A. Uddin, S. Zeb, Q. U. Hassan, Y. Gao, 3D porous superoleophilic/hydrophobic grapefruit peel aerogel for efficient removal of emulsified-oil from water, J. Environ. Chem. Eng. 11 (2023) 109324, https://doi.org/10.1016/j.jece.2023.109324.
- [19] G. Pandey, S. Singh, G. Hitkari, Synthesis and characterization of polyvinyl pyrrolidone (PVP)-coated Fe3O4 nanoparticles by chemical co-precipitation method and removal of Congo red dye by adsorption process, Int. Nano Lett. 8 (2018) 111–121, https://doi.org/10.1007/s40089-018-0234-6.
- [20] M.K. Purkait, S. DasGupta, S. De, Removal of dye from wastewater using micellar-enhanced ultrafiltration and recovery of surfactant, Sep. Purif. Technol. 37 (2004) 81–92, https://doi.org/10.1016/j.seppur.2003.08.005.
- [21] M.M. Hassan, C.M. Carr, A critical review on recent advancements of the removal of reactive dyes from dyehouse effluent by ion-exchange adsorbents, Chemosphere 209 (2018) 201–219, https://doi.org/10.1016/j.chemosphere.2018.06.043.
- [22] H. Hosseini, S.M. Mousavi, Bacterial cellulose/polyaniline nanocomposite aerogels as novel bioadsorbents for removal of hexavalent chromium: experimental and simulation study, J. Clean. Prod. 278 (2021) 123817, https://doi.org/10.1016/j. iclepro.2020.123817.
- [23] C.B. Godiya, X. Cheng, D. Li, Z. Chen, X. Lu, Carboxymethyl cellulose/ polyacrylamide composite hydrogel for cascaded treatment/reuse of heavy metal ions in wastewater, J. Hazard. Mater. 364 (2019) 28–38, https://doi.org/10.1016/ i.ihazmat.2018.09.076.
- [24] P. Wang, M. Cao, C. Wang, Y. Ao, J. Hou, J. Qian, Kinetics and thermodynamics of adsorption of methylene blue by a magnetic graphene-carbon nanotube composite, Appl. Surf. Sci. 290 (2014) 116–124, https://doi.org/10.1016/j.
- [25] S. Ye, M. Cheng, G. Zeng, X. Tan, H. Wu, J. Liang, M. Shen, B. Song, J. Liu, H. Yang, Y. Zhang, Insights into catalytic removal and separation of attached metals from natural-aged microplastics by magnetic biochar activating oxidation process, Water Res. 179 (2020) 115876, https://doi.org/10.1016/j.watres.2020.115876.
- [26] T. Huang, M. Yan, K. He, Z. Huang, G. Zeng, A. Chen, M. Peng, H. Li, L. Yuan, G. Chen, Efficient removal of methylene blue from aqueous solutions using magnetic graphene oxide modified zeolite, J. Colloid Interface Sci. 543 (2019) 43–51, https://doi.org/10.1016/j.jcis.2019.02.030.
- [27] S.D.K. Seera, D. Kundu, P. Gami, P.K. Naik, T. Banerjee, Synthesis and characterization of xylan-gelatin cross-linked reusable hydrogel for the adsorption

- of methylene blue, Carbohydr. Polym. 256 (2021) 117520, https://doi.org/
- [28] F. Ren, Z. Li, W.Z. Tan, X.H. Liu, Z.F. Sun, P.G. Ren, D.X. Yan, Facile preparation of 3D regenerated cellulose/graphene oxide composite aerogel with high-efficiency adsorption towards methylene blue, J. Colloid Interface Sci. 532 (2018) 58–67, https://doi.org/10.1016/j.jcis.2018.07.101.
- [29] A.B. Albadarin, M.N. Collins, M. Naushad, S. Shirazian, G. Walker, C. Mangwandi, Activated lignin-chitosan extruded blends for efficient adsorption of methylene blue, Chem. Eng. J. 307 (2017) 264–272, https://doi.org/10.1016/j. cei.2016.08.089.
- [30] X. Liu, Q. Wei, Removal of methylene blue from aqueous solution using porous starch:: G -poly(acrylic acid) superadsorbents, RSC Adv. 6 (2016) 79853–79858, https://doi.org/10.1039/c6ra14903k.
- [31] T. Jiang, Z. Guo, W. Liu, Biomimetic superoleophobic surfaces: focusing on their fabrication and applications, J. Mater. Chem. A 3 (2015) 1811–1827, https://doi. org/10.1039/c4ta05582a
- [32] L. Wen, Y. Tian, L. Jiang, Bioinspired super-wettability from fundamental research to practical applications, Angew. Chem. Int. Ed. 54 (2015) 3387–3399, https://doi. org/10.1002/anie.201409911.
- [33] L. Wu, L. Li, B. Li, J. Zhang, A. Wang, Magnetic, durable, and superhydrophobic polyurethane@Fe304@Si02@fluoropolymer sponges for selective oil absorption and oil/water separation, ACS Appl. Mater. Interfaces 7 (2015) 4936–4946, https://doi.org/10.1021/am5091353.
- [34] S. Zhou, G. Hao, X. Zhou, W. Jiang, T. Wang, N. Zhang, L. Yu, One-pot synthesis of robust superhydrophobic, functionalized graphene/polyurethane sponge for effective continuous oil-water separation, Chem. Eng. J. 302 (2016) 155–162, https://doi.org/10.1016/j.cej.2016.05.051.
- [35] J. Yang, H. Song, X. Yan, H. Tang, C. Li, Superhydrophilic and superoleophobic chitosan-based nanocomposite coatings for oil/water separation, Cellulose 21 (2014) 1851–1857, https://doi.org/10.1007/s10570-014-0244-0.
- [36] E. Hu, S. Shang, X. ming Tao, S. Jiang, K. lok Chiu, Regeneration and reuse of highly polluting textile dyeing effluents through catalytic ozonation with carbon aerogel catalysts, J. Clean. Prod. 137 (2016) 1055–1065, https://doi.org/10.1016/ j.jclepro.2016.07.194.
- [37] S. Kabiri, D.N.H. Tran, S. Azari, D. Losic, Graphene-diatom silica aerogels for efficient removal of mercury ions from water, ACS Appl. Mater. Interfaces 7 (2015) 11815–11823, https://doi.org/10.1021/acsami.5b01159.
- [38] C. Su, H. Yang, S. Song, B. Lu, R. Chen, A magnetic superhydrophilic/oleophobic sponge for continuous oil-water separation, Chem. Eng. J. 309 (2017) 366–373, https://doi.org/10.1016/j.cej.2016.10.082.
- [39] M. Zhang, J. Cui, T. Lu, G. Tang, S. Wu, W. Ma, C. Huang, Robust, functionalized reduced graphene-based nanofibrous membrane for contaminated water purification, Chem. Eng. J. 404 (2021), https://doi.org/10.1016/j. cei.2020.126347.
- [40] Y. Wang, L. Zhu, F. Zhu, L. You, X. Shen, S. Li, Removal of organic solvents/oils using carbon aerogels derived from waste durian shell, J. Taiwan Inst. Chem. Eng. 78 (2017) 351–358, https://doi.org/10.1016/j.jtice.2017.06.037.
- [41] L. Segal, J.J. Creely, A.E. Martin, C.M. Conrad, An empirical method for estimating the degree of crystallinity of native cellulose using the X-ray diffractometer, Textil. Res. J. 29 (1959) 786–794, https://doi.org/10.1177/004051755902901003.
- [42] Y. Ding, Z. Tian, H. Li, X. Wang, Efficient removal of organic dyes using a three-dimensional graphene aerogel with excellent recycling stability, N. Carbon Mater. 34 (2019) 315–324, https://doi.org/10.1016/S1872-5805(19)30020-4.
- [43] G. Kresse, J. Furthmüller, Efficiency of ab-initio total energy calculations for metals and semiconductors using a plane-wave basis set, Comput. Mater. Sci. 6 (1996) 15–50, https://doi.org/10.1016/0927-0256(96)00008-0.
- [44] G. Kresse, Efficient iterative schemes for ab initio total-energy calculations using a plane-wave basis set, Phys. Rev. B (n.d.) 169–196. https://doi.org/10.110 3/PhysRevB.54.11169.
- [45] G. Kresse, From ultrasoft pseudopotentials to the projector augmented-wave method, Phys. Rev. B (n.d.) 1758–1775. https://doi.org/10.1103/PhysRevB.59.1 758.
- [46] M Ernzerhof, J.P Perdew, K Burke, Generalized Gradient Approximation Made Simple, Phys. Rev. Lett. (.) 3865–3868. https://doi.org/10.1103/PhysRevLett 77, 3865
- [47] J.D. Pack, H.J. Monkhorst, "special points for Brillouin-zone integrations"-a reply, Phys. Rev. B 16 (1977) 1748–1749, https://doi.org/10.1103/PhysRevB.16.1748.
- [48] K. Mathew, R. Sundararaman, K. Letchworth-Weaver, T.A. Arias, R.G. Hennig, Implicit solvation model for density-functional study of nanocrystal surfaces and reaction pathways, J. Chem. Phys. 140 (2014), https://doi.org/10.1063/ 1.4865107.
- [49] A.V. Marenich, C.J. Cramer, D.G. Truhlar, Universal solvation model based on solute electron density and on a continuum model of the solvent defined by the bulk dielectric constant and atomic surface tensions, J. Phys. Chem. B 113 (2009) 6378–6396, https://doi.org/10.1021/jp810292n.
- [50] K.S. William Humphrey, Andrew Dalke, VMD: Visual Molecular Dynamics, J. Mol. Graph. (n.d.) 33–38. https://doi.org/10.1016/0263-7855(96)00018-5.
- [51] T. Lu, F. Chen, Multiwfn: a multifunctional wavefunction analyzer, J. Comput. Chem. 33 (2012) 580–592, https://doi.org/10.1002/jcc.22885.
- [52] K. Kinashi, Y. Kambe, M. Misaki, Y. Koshiba, K. Ishida, Y. Ueda, Synthesis, characterization, photo-induced alignment, and surface orientation of poly(9,9-dioctylfluorene-alt-azobenzene)s, J. Polym. Sci. Part A Polym. Chem. 50 (2012) 5107–5114, https://doi.org/10.1002/pola.26338.
- [53] I. Imae, T. Mashima, H. Sagawa, K. Komaguchi, Y. Ooyama, Y. Harima, In situ conductivity measurements of polythiophene partially containing 3,4-

- ethylenedioxythiophene and 3-hexylthiophene, J. Solid State Electrochem. 19 (2015) 71–76, https://doi.org/10.1007/s10008-014-2579-8.
- [54] T. Darmanin, F. Guittard, Superoleophobic surfaces with short fluorinated chains? Soft Matter 9 (2013) 5982–5990, https://doi.org/10.1039/c3sm50643f.
- [55] V.H. Pham, J.H. Dickerson, Superhydrophobic silanized melamine sponges as high efficiency oil absorbent materials, ACS Appl. Mater. Interfaces 6 (2014) 14181–14188, https://doi.org/10.1021/am503503m.
- [56] T. Darmanin, F. Guittard, Wettability of conducting polymers: from superhydrophilicity to superoleophobicity, Prog. Polym. Sci. 39 (2014) 656–682, https://doi.org/10.1016/j.progpolymsci.2013.10.003.
- [57] G. Sailakshmi, T. Mitra, A. Gnanamani, Engineering of chitosan and collagen macromolecules using sebacic acid for clinical applications, Prog. Biomater. 2 (2013) 1–12, https://doi.org/10.1186/2194-0517-2-11.
- [58] A. Tuteja, W. Choi, J.M. Mabry, G.H. McKinley, R.E. Cohen, Designing Superoleophobic Surfaces with Fluoroposs, 2007 AIChE Annu, Meet, 2007, pp. 1618–1622.
- [59] J.A. Howarter, K.L. Genson, J.P. Youngblood, Wetting behavior of oleophobic polymer coatings synthesized from fluorosurfactant-macromers, ACS Appl. Mater. Interfaces 3 (2011) 2022–2030, https://doi.org/10.1021/am200255v.
- [60] X. Zhang, H. Niu, Y. Pan, Y. Shi, Y. Cai, Chitosan-coated octadecyl-functionalized magnetite nanoparticles: preparation and application in extraction of trace

- pollutants from environmental water samples, Anal. Chem. 82 (2010) 2363–2371, https://doi.org/10.1021/ac902589t.
- [61] C. Jin, S. Han, J. Li, Q. Sun, Fabrication of cellulose-based aerogels from waste newspaper without any pretreatment and their use for absorbents, Carbohydr. Polym. 123 (2015) 150–156, https://doi.org/10.1016/j.carbpol.2015.01.056.
- [62] Y. Li, X. Luo, S. Yang, X. Cao, Z. Wang, W. Shi, S. Zhang, High specific monoclonal antibody production and development of an ELISA method for monitoring T-2 toxin in rice, J. Agric. Food Chem. 62 (2014) 1492–1497, https://doi.org/ 10.1021/jf404818r.
- [63] J. Wang, H. Wang, Ultra-hydrophobic and mesoporous silica aerogel membranes for efficient separation of surfactant-stabilized water-in-oil emulsion separation, Sep. Purif. Technol. 212 (2019) 597–604, https://doi.org/10.1016/j. seppur.2018.11.078.
- [64] W. Wan, R. Zhang, W. Li, H. Liu, Y. Lin, L. Li, Y. Zhou, Graphene-carbon nanotube aerogel as an ultra-light, compressible and recyclable highly efficient absorbent for oil and dyes, Environ. Sci. Nano 3 (2016) 107–113, https://doi.org/10.1039/ c5en00125k.
- [65] R. Li, C. Chen, J. Li, L. Xu, G. Xiao, D. Yan, A facile approach to superhydrophobic and superoleophilic graphene/polymer aerogels, J. Mater. Chem. A 2 (2014) 3057–3064, https://doi.org/10.1039/c3ta14262k.